How to cite: *Angew. Chem. Int. Ed.* **2021**, *60*, 4090–4097
International Edition: doi.org/10.1002/anie.202011482
German Edition: doi.org/10.1002/ange.202011482

Batteries **Hot Paper**

Regulating Interfacial Chemistry in Lithium-Ion Batteries by a Weakly Solvating Electrolyte**

*Yu-Xing Yao, Xiang Chen, Chong Yan, Xue-Qiang Zhang, Wen-Long Cai, Jia-Qi Huang, and Qiang Zhang**

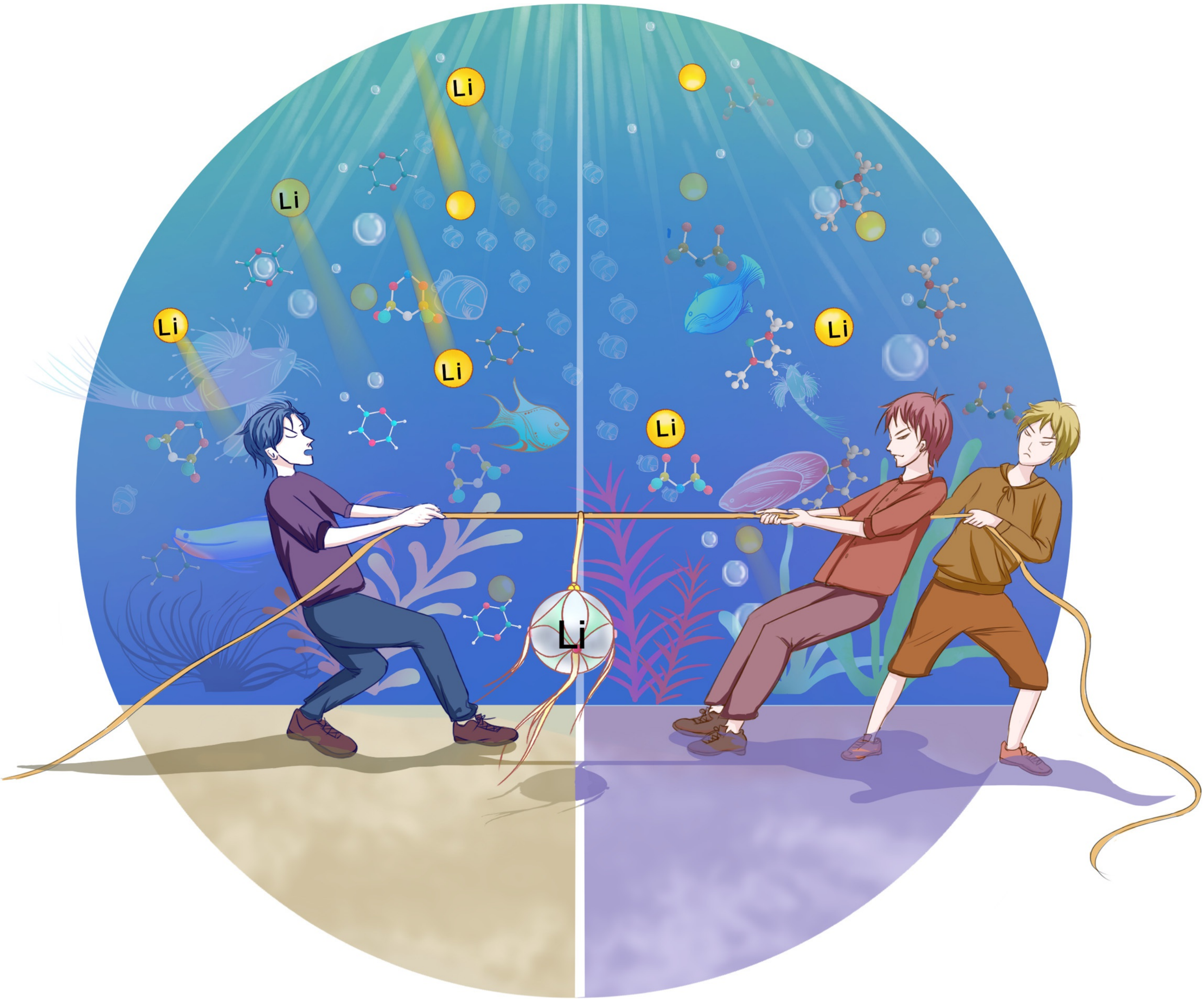

Abstract: *The performance of Li-ion batteries (LIBs) is highly dependent on their interfacial chemistry, which is regulated by electrolytes. Conventional electrolyte typically contains polar solvents to dissociate Li salts. Herein we report a weakly solvating electrolyte (WSE) that consists of a pure non-polar solvent, which leads to a peculiar solvation structure where ion pairs and aggregates prevail under a low salt concentration of 1.0 M. Importantly, WSE forms unique anion-derived interphases on graphite electrodes that exhibit fast-charging and long-term cycling characteristics. First-principles calculations unravel a general principle that the competitive coordination between anions and solvents to Li ions is the origin of different interfacial chemistries. By bridging the gap between solution thermodynamics and interfacial chemistry in batteries, this work opens a brand-new way towards precise electrolyte engineering for energy storage devices with desired properties.*

Introduction

The Nobel Prize in Chemistry 2019 finally rewarded the development of Li-ion batteries (LIBs). These lightweight, rechargeable, and ubiquitous energy storage devices have profoundly revolutionized our modern life during the past 30 years.[1] The increasing demands of electric vehicles and grid energy storage is gradually pushing the performance of LIBs to their limits, including high energy density, fast-charging, high safety, long life, and low cost.[2] To meet these high bars, current LIBs must venture into more challenging territories such as Li/Si anodes,[3] high-voltage/capacity cathodes,[4] and aqueous LIBs.[5] Eventually, the challenges for these aggressive battery chemistries are partially or completely passed on to designing advanced electrolytes.[6] The electrolytes in LIBs not only serve as an ionic conductor, but also largely determine the electrode/electrolyte interfacial chemistry.[7] The exploration of state-of-the-art electrolytes is essential to achieve to the high expectations of working rechargeable batteries since the performance of LIBs is strongly dependent on the electrode/electrolyte interfaces.

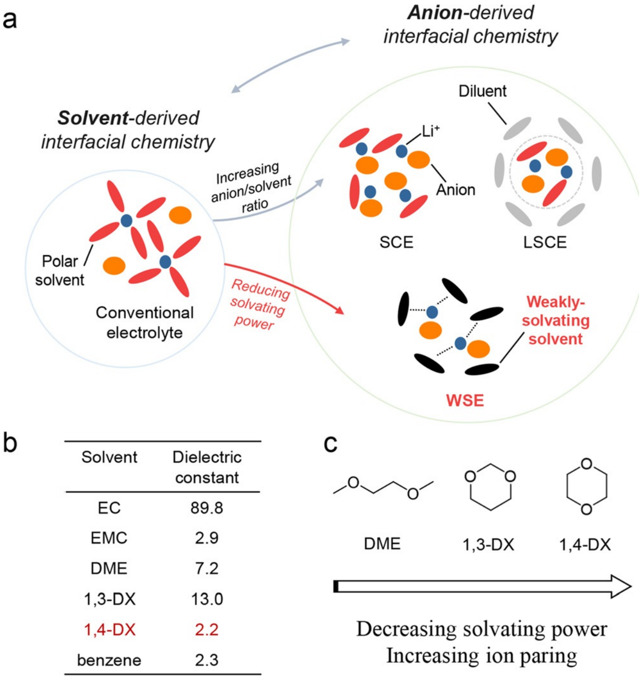

Solvent	Dielectric constant
EC	89.8
EMC	2.9
DME	7.2
1,3-DX	13.0
1,4-DX	2.2
benzene	2.3

Figure 1. a) The solvation structures in conventional electrolyte, superconcentrated electrolyte (SCE), localized superconcentrated electrolyte (LSCE), and weakly solvating electrolyte (WSE). b) Dielectric constant of various solvents. c) The ranking of solvating power of solvents from high to low.

It is well-established that the interfacial chemistry on electrodes is closely correlated to the solvation structure of electrolytes. In conventional dilute electrolytes, Li ions are usually solvated by strongly solvating polar solvents and most anions are excluded from the solvation sheath (Figure 1 a).[7,8] Since the primary solvation sheath is the precursor of solid electrolyte interphase (SEI), such solvation structure leads to solvent-derived interfacial chemistry.[9] For example, the indispensable role of ethylene carbonate (EC) in modern LIBs originates from its preferential solvation and reduction which creates an exclusive EC-derived SEI to support reversible Li^+ intercalation in graphite. One major innovation of unconventional electrolytes in the past decade is the concept of superconcentrated electrolyte (SCE), with salt concentration (>3.0 M) far beyond conventional electrolytes (≈ 1.0 M, required by the optimum conductivity).[10] Unlike the solvent-dominated solvation structure in dilute electrolytes, anions inevitably appear in the primary solvation sheath of Li^+ to form ion pairs or aggregates because of the scarcity of solvents and abundance of anions (Figure 1 a).[11,12] Such solvation structure leads to anion-derived SEI that enables high-rate and long-term cycling of graphite and Li metal electrodes.[13] Considering the high cost and viscosity of SCE, diluting SCE with non-polar solvents emerged in recent years as an alternative to mitigate these issues.[14,15] The diluted SCE is termed localized superconcentrated electrolytes (LSCE) because the local solvation structure of LSCE is very similar to that of SCE, and therefore they belong to the same methodology.

Because solvent and anion can both serve as ligands to coordinate with Li^+ through ion-dipole or ion-ion interactions, the actual solvation structure depends on the competitive coordination between them.[16] In dilute electrolytes, solvents usually outnumber anions and hence dominate the solvation sheath of Li^+. To achieve anion-derived interfacial chemistry, the straightforward strategy is to increase the ratio of anion to solvent as in SCE or LSCE (Figure 1 a). However,

---

[*] Y.-X. Yao, X. Chen, Dr. C. Yan, X.-Q. Zhang, Dr. W.-L. Cai, Prof. Q. Zhang
Beijing Key Laboratory of Green Chemical Reaction Engineering and Technology, Department of Chemical Engineering
Tsinghua University, Beijing 100084 (China)
E-mail: zhang-qiang@mails.tsinghua.edu.cn
Dr. C. Yan, Prof. J.-Q. Huang
Advanced Research Institute of Multidisciplinary Science
Beijing Institute of Technology, Beijing 100081 (China)

[**] A previous version of this manuscript has been deposited on a preprint server (https://doi.org/10.21203/rs.3.rs-46256/v1).
Supporting information and the ORCID identification number(s) for the author(s) of this article can be found under: https://doi.org/10.1002/anie.202011482.

is this the only way towards anion-derived interfacial chemistry?

A more essential approach towards anion-derived interfacial chemistry involves tuning the intrinsic solvating power of solvents. Because solvents and anions are competing to enter the solvation sheath of Li^+, reducing the solvating power of solvents can theoretically allow more anions to coordinate with Li^+. The ideal scenario (Figure 1 a) is a weakly solvating electrolyte (WSE) that generates abundant ion pairs or aggregates under low salt concentrations. While SCE and LSCE are extensively studied, WSE is rarely visited because solvents with low solvating power usually can not even dissolve enough Li salts.[14,16] This contradiction therefore has left this area blank, with some potentially important concepts and theories of electrolyte undiscovered.

In this work, we successfully prepared a WSE and systematically studied its solvation structure as well as interfacial chemistry on electrodes. Particularly, ultra-low solvating power and moderate Li salt solubility are simultaneously achieved in a specific solvent (1,4-dioxane) despite the apparent contradiction. Spectroscopic results confirm that WSE exhibits a peculiar solvation structure, in which ion pairs and aggregates prevail under a standard Li salt concentration of 1.0 M. Such solvation structure leads to an anion-derived, inorganic-rich SEI on graphite electrode, which allows for fast Li^+ transport. First-principles calculations unravel a fundamental rationale that the relative binding energy between anions/solvents and Li^+ dictates the electrode/electrolyte interfacial chemistry, which blazes a new trail in precise electrolyte design for future batteries.

Results and Discussion

Model System

Figure 1 b lists the dielectric constant (ε, also known as permittivity) of various solvents used in this study, which is an important indicator of the solvating power of solvents. Another frequently used indicator, donor number (DN), is also provided for a list of solvents (Supporting Information, Table S1) along with a detailed discussion on the applicability of these two parameters. In the carbonate family, EC possesses an extremely high ε of 89.8 as a strongly solvating solvent and dominates the primary solvation sheath of Li^+. The Li^+-coordinated EC is then reduced on graphite electrode to form a desirable SEI, which is contributed by the typical solvent-derived interfacial chemistry. In this study, commercial electrolyte consisting of EC/ethyl methyl carbonate (EMC; 1:2, v/v) mixed solvents and 1.0 M lithium bis(fluorosulfonyl)imide (LiFSI) serves as the control sample and is denoted as EC/EMC. Three ethers, dimethoxyethane (DME), 1,3-dioxane (1,3-DX), and 1,4-dioxane (1,4-DX) with ε of 7.0, 13.0, and 2.2, respectively, are chosen as the model system to induce a transition from solvent-derived interfacial chemistry to anion-derived interfacial chemistry based on solvating power regulation (Figure 1 c). DME has the largest solvating power among the three solvents despite the moderate ε, because it has a high donor number ($DN = 20.0$) and chelating effect on Li^+.[17] 1,3-DX exhibits lower solvating power due to the steric effect caused by its cyclic structure. The most extreme case and the protagonist in this study, 1,4-DX, possesses an ultra-low ε even lower than that of benzene ($\varepsilon = 2.3$), which are both typical non-polar solvents. Theoretically, 1,4-DX should have an extremely weak solvating power. Actually, lithium hexafluorophosphate ($LiPF_6$) is almost insoluble in 1,4-DX,and lithium bis(trifluoromethylsulfonyl)imide (LiTFSI) also exhibits a very limited solubility (< 0.3 M) although these two salts possess a high solubility and are commonly adopted in battery research and industrial applications (Supporting Information, Figure S1a,b). Interestingly, lithium bis(fluorosulfonyl)imide (LiFSI) is found to be the only soluble Li salt in 1,4-DX, exhibiting a maximum solubility up to 2.0 M (Supporting Information, Figure S1c) and conceivably forming a unique solvation structure. More discussions on the solvating power of these solvents are given in the supporting information. To ensure that solvating power is the only controlled variable in this study, all electrolytes were formulated with 1.0 M LiFSI as Li salt and denoted as the name of their solvents. The elaborately designed electrolyte series, namely DME, 1,3-DX, and 1,4-DX, should represent a decreasing trend of solvating power and increasing trend of ion pair formation.

Solvation Structure

The solvation structures of the above-mentioned electrolytes were investigated by spectroscopic characterizations combined with first-principles calculations. Raman spectra were firstly obtained for three ether-based electrolytes (Figure 2 a; Supporting Information, Figure S2). As shown in Figure 2 a, The S–N–S bending signal in FSI^- anion can be classified into three distinctive bands: free anion (FA, 719.0 cm^{-1}, non-coordinated FSI^-), contact ion pair (CIP, 730.6 cm^{-1}, one FSI^- binding with one Li^+), and ion aggregate (AGG, 742.3 cm^{-1}, one FSI^- binding with two or more Li^+).[18] The specific portion of these three species were calculated from the peak area and listed in Figure 2 b.[12] DME electrolyte contains 71.3 % of FA, 28.7 % CIP, and no AGG, indicating that most anions are expelled from the primary solvation sheath due to the strong solvating power of DME. The dissociation degree of LiFSI, α, is 71.3 % in this case. Accordingly, a new vibration band of DME solvent at 800–900 cm^{-1} arises (Supporting Information, Figure S2a), which signifies the abundant Li^+–DME complexes. In 1,3-DX with less solvating power, the ratio of FA significantly reduces as the ratio of CIP and AGG increases. The additional band of 1,3-DX vibration (Supporting Information, Figure S2b) indicates that considerable Li^+–1,3-DX complexes are still present. Surprisingly, the weakly solvating 1,4-DX electrolyte contains merely 15.6 % of FA ($\alpha = 15.6\%$), and the solvation structure is dominated by CIP (49.0 %) and AGG (35.4 %). Raman vibration bands of pure 1,4-DX and 1.4-DX electrolyte are almost identical (Supporting Information, Figure S2b), indicating that the interaction between 1,4-DX and Li^+ is extremely weak. Nevertheless, the solubility of LiFSI in 1,4-DX is sufficiently high. This counterintuitive

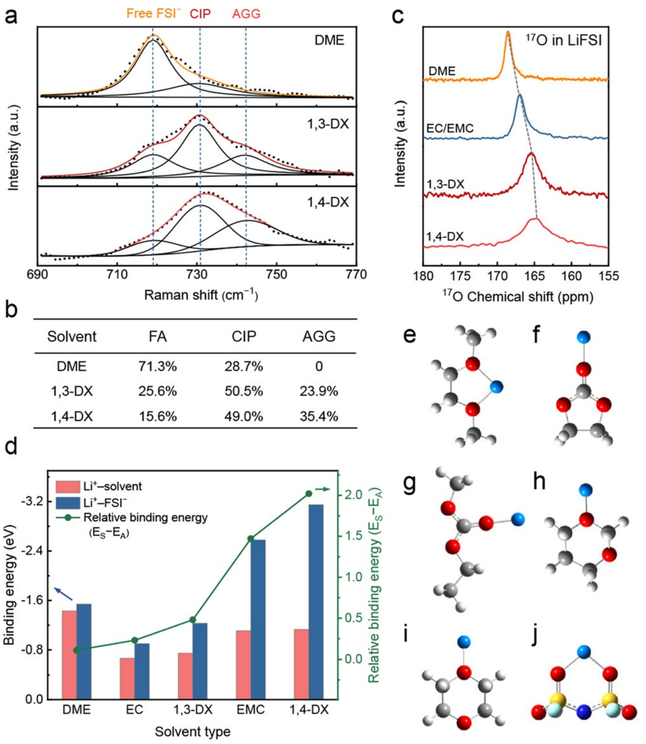

Solvent	FA	CIP	AGG
DME	71.3%	28.7%	0
1,3-DX	25.6%	50.5%	23.9%
1,4-DX	15.6%	49.0%	35.4%

Figure 2. The evolution of solvation structure by regulating the solvating power of solvents. a) Raman spectra of 1.0 M LiFSI dissolved in various solvents. b) The ratio of different solution structures in various solvents calculated from (a). c) Natural-abundance ^{17}O NMR spectra of 1.0 M LiFSI dissolved in various solvents. Signals were collected at 60 °C. d) The binding energies between Li^+ and solvents/anions obtained by first-principles calculations. The corresponding optimized geometrical structures of e) Li^+–DME, f) Li^+–EC, g) Li^+–EMC, h) Li^+–1,3-DX, i) Li^+–1,4-DX, j) Li^+–FSI^-. H white, Li blue, C gray, O red, S yellow, N dark blue, F light blue.

result suggests that LiFSI becomes a weak electrolyte and largely undissociated in sparingly solvating 1,4-DX solvent, although it is regarded as a strong electrolyte in conventional solvents owing to the very weak interaction between Li^+ and charge-delocalized FSI^-.

The ^{17}O nuclear magnetic resonance spectroscopy (^{17}O-NMR) analysis confirms the same trend of transition of the solvation structure (Figure 2c; Supporting Information, Figure S3). When the lone pair electrons in anions or solvents coordinate with Li^+, it results in a shielding effect on the electronic environment of ^{17}O nuclei which is subsequently expressed by the upfield displacement of chemical shifts in NMR spectra.[19] The chemical shift of ^{17}O nuclei in LiFSI molecules decreases in the order of DME > EC/EMC > 1,3-DX > 1,4-DX, indicating that the coordination strength between Li^+ and FSI^- follows the reverse trend. The above preliminary results show that a WSE is indeed constructed exactly as designed when LiFSI is dissolved in 1,4-DX. As a direct correlation, when the solvating power of solvent reduces, solvents in the primary solvation sheath are gradually replaced by anions.

To elucidate the origin of different solvation structures, first-principles calculations were further conducted to probe the molecular interactions between anions/solvents and Li^+ (Figure 2d–j; Supporting Information, Table S2), which are expressed in terms of binding energy. The binding energy of Li^+–solvent (E_S) and Li^+–anion (E_A) complexes is primarily determined by two major factors: 1) The chemical structure of the ligands. Typically, carbonyl O exhibits higher nucleophilicity than ethereal O; therefore, carbonates usually have higher solvating power than ethers. Moreover, ligands with multiple coordination sites (also known as the chelating effect) exhibit stronger interaction with Li^+ than monodentate ligands. For example, DME and FSI^- both have two O atoms to coordinate with Li^+ (Figure 2e and j), therefore exhibit larger binding energies (for example, $E_S = -1.43$ eV for DME). The coulombic attraction between Li^+ and FSI^- contributes to an even stronger interaction and thus larger E_A compared to E_S. 2) The dielectric constant of the solution. Large dielectric constant of solvents weakens the Li^+–anion and Li^+–solvent interactions, which can be approximately described by classical physical models:[16]

$$U_{ion-ion} = \frac{-1}{4\pi\varepsilon} \times \frac{q_1 q_2}{r} \tag{1}$$

$$U_{ion-dipole} = \frac{-1}{4\pi\varepsilon} \times \frac{q\mu cos\theta}{r^2} \tag{2}$$

where ε is the dielectric constant, q the charge of ion, μ the dipole moment of dipole, r the distance between ion and ion or ion and the center of dipole, and θ the dipole angle relative to the line r joining the ion and the center of the dipole. For instance, the relatively low E_S of EC (-0.67 eV, which seems contradictory to its high solvating power) is due to its large ε (89.8), and the extremely high E_A (-3.15 eV) in 1,4-DX is due to its small ε (2.2) that inhibits salt dissociation. Interestingly, if the binding energy of Li^+–EC is calculated in 1,4-DX environment (which practically means to add a small amount of EC in 1,4-DX that does not change the solvent environment), the E_S of Li^+–EC (-1.38 eV) is significantly larger than the E_S of Li^+–1,4-DX (-1.13 eV). According to the above analyses, it is unreasonable to directly compare E_S–E_A in different electrolytes because it does not reveal direct information on the solvation structure of an electrolyte. On the other hand, analyzing the value of E_S and E_A in the same electrolyte environment affords fresh insights on the competitive coordination between anions and solvents with Li^+.

The descriptor of E_S–E_A is further proposed to predict the actual solvation structure in different electrolytes. A larger E_S–E_A indicates that the ion pair and aggregate are preferentially formed over Li^+–solvent complexes, namely that anions win the coordination competition over solvents. Figure 2d illustrates that the trend of E_S–E_A (DME < EC < 1,3-DX < 1,4-DX) is in perfect accordance with spectroscopic results, which strongly affirms the applicability of the descriptor of E_S–E_A. As a rule of thumb, large numbers of Li^+–solvent complexes and free anions are anticipated for E_S–E_A close to 0 (such as in DME); ion pairs and aggregates prevail for extremely large E_S–E_A (> 2.0 eV, such as in 1,4-DX); Li^+–solvent complex and ion pair jointly constitute the solvation structure for intermediate E_S–E_A (0.5–1.5 eV, such as in 1,3-DX). The most striking significance to emerge from

E_S–E_A is that it serves as a quantitative indicator to predict to what extent do anions intrude the primary solvation sheath of Li^+. Our theory reveals the underlying mechanism that different solvation structures originate from the competitive coordination between solvents and anions towards a thermodynamically stable Li^+ solvation sheath.

Li^+ Intercalation Behavior in Graphite

To explore the effect of different solvation structures on the interfacial chemistry of electrodes, graphite electrode is chosen as a touchstone because the reversible Li^+ intercalation in graphite is highly sensitive to the solvation structure of Li^+ in bulk electrolyte.[20] Figure 3 a,b exhibits the charge/discharge curves and cyclic voltammetry (CV) curves of graphite during the first cycle in different electrolytes. EC is strongly coordinated with Li^+ and reduced at about 0.8 V vs. Li/Li^+ to form a stable SEI in the EC/EMC electrolyte (Supporting Information, Figure S4), which is a typical case of solvent-derived interfacial chemistry. Graphite lithiation/delithiation in EC/EMC is highly reversible, with three voltage plateaus between 0.05–0.25 V representing the different stages of Li-graphite intercalation compounds. Unlike carbonates, ethers have long been regarded as unstable against graphite electrode.[7] DME electrolyte causes severe co-intercalation at 0.4–1.0 V that undermines the structure of layered graphite (Supporting Information, Figure S5) so that reversible lithiation cannot be achieved. This is because DME are also strongly coordinated with Li^+ but is unable to form stable SEI that prevents co-intercalation. This phenomenon is common for ether-based electrolytes, as 1,3-DX also exhibits slight co-intercalation, sluggish lithiation kinetics, and an initial coulombic efficiency (ICE) of merely 68.03 %. Although the co-intercalation of 1,3-DX is milder than that of DME because of the weaker solvating power and higher degree of ion pair formation (Supporting Information, Figure S5), the reversibility of graphite lithiation is still unsatisfactory. Surprisingly, 1,4-DX electrolyte exhibits a high reversible capacity of 360.5 mAh g^{-1} and faster lithiation/delithiation kinetics even exceeding the commercial EC/EMC electrolyte. The ICE of 1,4-DX (86.7 %) is close to that of EC/EMC (88.94 %), implying that 1,4-DX electrolyte leads to a stable SEI formation. To the best of our knowledge, this is the first report of highly reversible lithiation of graphite in neat ether electrolytes without applying superconcentration or any additives. This unexpected phenomenon is attributed to the unique solvation structure of the 1,4-DX electrolyte, where the prevailing ion pairs and aggregates leads to preferential reduction of anions (at about 1.0 V; Figure 3 b; Supporting Information, Figure S4) to form an anion-derived SEI. To verify this postulation, a detailed investigation on the SEI of graphite is requested.

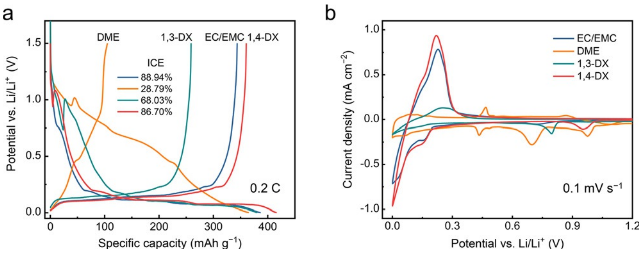

Figure 3. Electrochemical behavior of graphite electrodes in various neat solvents containing 1.0 M LiFSI. a) First cycle charge-discharge curves and b) first-cycle CV curves of graphite electrodes in various electrolytes.

Interfacial Chemistry and Kinetics

The surface passivation film on graphite (SEI) is the key to reversible Li^+ intercalation.[21] The Li^+ intercalation behavior of graphite indicates that only two electrolytes can form stable SEI and enable reversible lithiation: the commercial EC/EMC electrolyte and the 1,4-DX electrolyte (also denoted as WSE). XPS is conducted to characterize the composition and structure of SEI on graphite in these two electrolytes and study the SEI formation mechanisms. The deconvolution of C 1s spectra reveals four peaks (Figure 4 a), representing C−C (284.8 eV, from graphite), C−O (286.6 eV), C=O (288.8 eV), and C−F (290.1 eV, from PVDF binder). The peak intensities of C−O and C=O in WSE are significantly lower than that of EC/EMC, indicating a suppressed solvent decomposition in WSE compared to the EC decomposition in EC/EMC that generates abundant organic species in SEI.

The atomic concentration at different etching depths reveals the structure of SEI (Figure 4 b,c). The etching depth corresponds to the standard thermal oxidation of SiO_2 samples. For EC/EMC, the C and O concentrations sharply decrease from 0 to 10 nm as the F content increases, then

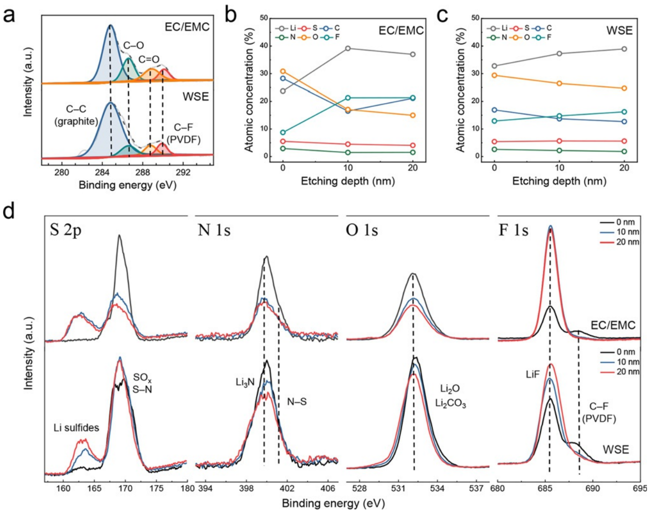

Figure 4. Interfacial chemistry of graphite electrodes in EC/EMC and WSE electrolyte revealed by XPS depth profiling after 5 formation cycles. a) C 1s spectra of SEI on graphite electrodes. Atomic concentration at different depths of SEI in b) EC/EMC electrolyte and c) WSE electrolyte. d) S 2p, N 1s, O 1s, and F 1s spectra of SEI on graphite electrodes at different depths.

stabilize from 10 to 20 nm. This result is in accordance with the classic two-layer SEI model, in which the outer layer mainly consists of organic species at higher oxidation state (mainly Li alkyl carbonates) and the inner layer consists of various inorganic compounds (LiF, Li_2CO_3, and N,S-containing species as shown in Figure 4 d) that are more stable against reduction.[22] Therefore, SEI is mainly solvent-derived in EC/EMC electrolytes, accompanied by partial anion reduction. In contrast, the atomic contents in WSE-derived SEI are almost constant from 0 to 20 nm with lower C content and more inorganic ingredients, indicating that the SEI is highly homogeneous along its depth and inorganic in nature. A closer examination reveals that the O content in WSE-derived SEI is roughly twice of the F content, which is exactly the stoichiometric ratio in FSI^-. Therefore, in WSE the SEI is generated mainly through anion reduction that generates abundant inorganic species such as LiF, Li_2O, Li_3N, Li sulfide, and Li oxysulfide (Figure 4 d), and so on. The XPS results confirm that EC/EMC features solvent-derived interfacial chemistry and WSE features anion-derived interfacial chemistry.

Temperature-dependent electrochemical impedance spectroscopy (EIS) were employed to determine the kinetics of different interfacial processes. Three-electrode setup using a Li@Cu reference electrode was implemented to accurately measure the impedance signal of graphite electrode without the complication of the Li counter electrode (Figure 5 a; Supporting Information, Figure S6a–c). Based on a well-established theory, the semicircle at mid-frequency region in the Nyquist plot represents the desolvation step of Li^+ (known as the charge-transfer impedance) and the semicircle at high-frequency region represents Li^+ transport through SEI (Figure 5 b).[23] The EIS spectra were fitted according to the classic Arrhenius law and activation energies of each interfacial process are obtained (Figure 5 b,c). WSE shows a slightly reduced Li^+ desolvation energy barrier ($E_{a,ct} = 48.2\ \mathrm{kJ\,mol^{-1}}$) compared to EC/EMC ($E_{a,ct} = 54.7\ \mathrm{kJ\,mol^{-1}}$). Since the Li^+–solvent interaction is much weaker in WSE than in EC/EMC as previously demonstrated, such reduction of Li^+ desolvation energy barrier may seem insignificant. However, since the Li^+–FSI^- interaction in WSE is much stronger than in EC/EMC, desolvation is mainly contributed by the dissociation of ion pairs and aggregates which is also energy-consuming.[24] Most importantly, the activation energy for Li^+ transport through SEI in WSE ($E_{a,\,SEI} = 26.6\ \mathrm{kJ\,mol^{-1}}$) is significantly lower than in EC/EMC ($E_{a,\,SEI} = 44.7\ \mathrm{kJ\,mol^{-1}}$). This is because the inorganic species dispersed in anion-derived SEI creates abundant phase boundaries and vacancies for rapid Li^+ diffusion, which prominently reduce the energy barrier. In the solvent-derived SEI, Li^+ undergoes pore diffusion in the outer layer, which requires a higher activation energy and renders limited kinetics. The kinetics analysis implies that the unique anion-derived interphase may potentially enable fast-charging characteristic.

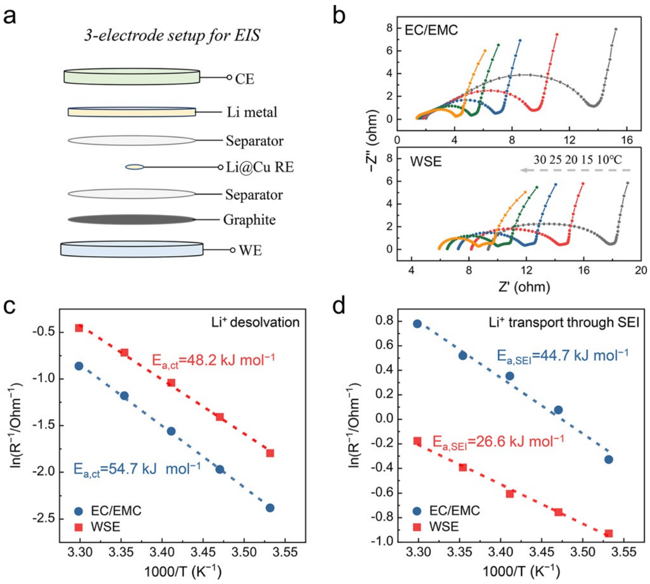

Figure 5. Kinetics of interfacial processes at the graphite/electrolyte interface measured by EIS using a 3-electrode setup. a) Cell configuration of 3-electrode setup for EIS measurements. b) Temperature-dependent EIS curves of cells containing EC/EMC and WSE. c) Arrhenius behavior of the resistance corresponding to Li^+ desolvation. d) Arrhenius behavior of the resistance corresponding to Li^+ transport through SEI.

Electrochemical Performance

To understand the role of different interfacial chemistries in the electrochemical performance of electrodes, both rate and cycling tests were conducted for graphite electrodes in EC/EMC and WSE electrolytes. The WSE exhibits a remarkable fast-charging performance even far exceeding the commercial EC/EMC electrolyte (Figure 6 a,b), retaining 54 % of its capacity even at a demanding rate of 4.0 C. The charging process can be divided into 4 steps: 1) Li^+ diffusion in the bulk electrolyte, especially in the micropores of the

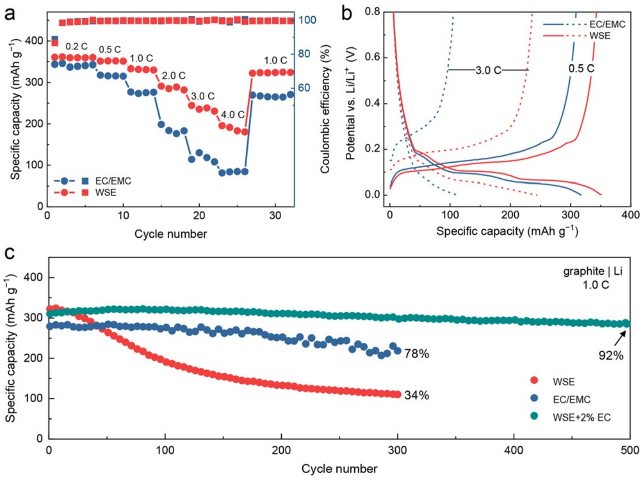

Figure 6. Electrochemical performance of graphite electrode in different electrolytes. a) Specific capacity of graphite electrodes in EC/EMC and WSE under various charge and discharge rates. b) The corresponding charge and discharge curves at selected rates. c) Long term cycling performance of graphite electrode in EC/EMC, WSE and WSE + 2 % EC electrolyte at 1.0 C charge and discharge rate. Long term cycling tests were conducted after the rate tests without interval.

graphite electrode; 2) Li^+ desolvation at the electrolyte/electrode interfaces; 3) Li^+ transport through SEI; and 4) Li diffusion within graphite galleries. It is obvious that process 4 is identical in EC/EMC and WSE. Because the ionic conductivity of WSE is nearly one-magnitude lower than that of EC/EMC (Supporting Information, Figure S7) due to the lack of Li salt dissociation, step 1 cannot be the reason for its outstanding rate performance. Consequently, the exceptional rate performance of WSE is attributed to the accelerated Li^+ desolvation step induced by its unique solvation structure, and rapid Li^+ diffusion through the anion-derived SEI. This conclusion is supported by the interfacial kinetics analysis. In other words, even the conductivity of WSE is substantially smaller, its anion-derived interfacial chemistry induces rapid kinetics of Li^+ migration across interfaces and the impressive fast-charging capability.

Long-term cycling of graphite electrodes at 1 C rate were carried out straight after the rate tests to examine the SEI stability (Figure 6c; Supporting Information, Figures S8a and S8b). EC/EMC exhibits a 78% capacity retention after 300 cycles, which is acceptable for routine EC-based electrolytes without any additive. However, WSE renders a rapid capacity decay during long term cycling and only retains 34% of its initial capacity after 300 cycles. This phenomenon is attributed to the fragile nature of inorganic-rich SEI derived from anion decomposition. The anion-derived SEI is broken under high stress due to the volume fluctuation of graphite during cycling. This leads to the repeated cracking and repair of SEI that gradually increase its thickness overtime, which finally result in a growing resistance and capacity fade. On the contrary, the organic SEI layer in EC/EMC possesses higher elasticity and is more resilient to mechanical deformations, therefore offers a better protection of the graphite electrode.

Interestingly, the fragility of anion-derived SEI and the poor cycling performance of WSE can be overcome by exploiting the competitive coordination between solvents and anions. As previously shown, the binding energy between Li^+ and EC is large in 1,4-DX environment (-1.38 eV; Supporting Information, Figure S4). Simply by adding 2.0 wt% EC into WSE (denoted as WSE + 2% EC), some EC molecules will coordinate with Li^+ and replace a small part of ion pairs and aggregates. Consequently, these EC molecules are reduced on graphite electrodes to produce a small number of organic compounds that infiltrate into the inorganic compounds, which serves as the glue to enhance the stability of SEI. As a result, WSE + 2% EC enables ultra-stable cycling of graphite electrode with 92% capacity retention after 500 cycles (Figure 6c; Supporting Information, Figure S8c), and retains a satisfactory rate performance (Supporting Information, Figure S9). If the cell was directly cycled at 1 C without the rate test, a longer life exceeding 840 cycles can be obtained with 80% capacity retention (Supporting Information, Figure S10). Such superior cycling performance is very rare for graphite electrodes in ether-based electrolytes, further demonstrating the huge potential of anion-derived interfacial chemistry achieved by solvating power regulation.

It is important to note that the aim of this work is not to demonstrate a practical electrolyte suitable for commercial LIBs, typically with high-voltage cathodes, high areal loading and wide-temperature range. For instance, the ether-based WSE is incompatible with high-voltage batteries, and the high melting point of 1,4-DX (11.8 °C) rules out low-temperature operation. Instead, a new concept in electrolyte is proposed, in which the methodology and underlying mechanism may inspire future electrolyte innovation towards more practical applications. Therefore, although electrochemical tests under practical conditions (such as full cell/pouch cell) are not provided herein, these preliminary results suggest that the concept of WSE bears huge potential for next-generation electrolyte systems for advanced LIBs. Future study may discover new solvents and lithium salts with better properties such as high anodic stability, wide liquid range, inhibition of Al dissolution and so on, for constructing WSEs with the potential to replace commercial EC-based electrolytes.

Conclusion

A completely new route towards anion-derived interfacial chemistry in LIBs is developed. Unlike superconcentrated electrolytes, the essence of this methodology is constructing a weakly solvating electrolyte by using a non-polar but salt-dissolving solvent. WSE exhibits a peculiar solvation structure where ion pairs and aggregates prevail under a low salt concentration of 1.0 M. As a result, the anion-derived SEI exhibits superior interfacial charge transport kinetics and high stability, enabling fast-charging and long-term cycling of graphite electrodes. First-principles calculations unravel the fundamental rationale that the competitive coordination between solvents and anions controls the transition from solvent-derived interfacial chemistry to anion-derived interfacial chemistry. Furthermore, a semi-empirical descriptor was put forward to predict the actual solvation structure in electrolytes. This work constitutes the first step of an undiscovered way towards anion-derived interfacial chemistry, in which the methodology serves as an emerging principle for coming studies on precise electrolyte engineering towards next-generation energy storage devices.

Acknowledgements

This work was supported by National Natural Science Foundation of China (21825501, 21805161, and U1801257), National Key Research and Development Program (2016YFA0202500), and the Tsinghua University Initiative Scientific Research Program. The authors thank Rui Xu and Lei Xu for useful discussions.

Conflict of interest

The authors declare no conflict of interest.

Keywords: batteries · electrolytes · graphite · interfacial chemistry · solvation

[1] C. Yan, R. Xu, Y. Xiao, J. F. Ding, L. Xu, B. Q. Li, J. Q. Huang, *Adv. Funct. Mater.* **2020**, *30*, 1909887; M. Li, J. Lu, Z. Chen, K. Amine, *Adv. Mater.* **2018**, *30*, 1800561; M. Winter, B. Barnett, K. Xu, *Chem. Rev.* **2018**, *118*, 11433 – 11456.

[2] J. Deng, C. Bae, A. Denlinger, T. Miller, *Joule* **2020**, *4*, 511 – 515; X. Q. Zeng, M. Li, D. Abd El-Hady, W. Alshitari, A. S. Al-Bogami, J. Lu, K. Amine, *Adv. Energy Mater.* **2019**, *9*, 1900161; R. Schmuch, R. Wagner, G. Horpel, T. Placke, M. Winter, *Nat. Energy* **2018**, *3*, 267 – 278; G. L. Zhu, C. Z. Zhao, J. Q. Huang, C. He, J. Zhang, S. Chen, L. Xu, H. Yuan, Q. Zhang, *Small* **2019**, *15*, 1805389; Q. Zhao, S. Stalin, C.-Z. Zhao, L. A. Archer, *Nat. Rev. Mater.* **2020**, *5*, 229 – 252.

[3] J. Liu, Z. Bao, Y. Cui, E. J. Dufek, J. B. Goodenough, P. Khalifah, Q. Li, B. Y. Liaw, P. Liu, A. Manthiram, Y. S. Meng, V. R. Subramanian, M. F. Toney, V. V. Viswanathan, M. S. Whittingham, J. Xiao, W. Xu, J. Yang, X.-Q. Yang, J.-G. Zhang, *Nat. Energy* **2019**, *4*, 180 – 186; X. B. Cheng, R. Zhang, C. Z. Zhao, Q. Zhang, *Chem. Rev.* **2017**, *117*, 10403 – 10473; K. Feng, M. Li, W. Liu, A. G. Kashkooli, X. Xiao, M. Cai, Z. Chen, *Small* **2018**, *14*, 1702737.

[4] W. Li, B. Song, A. Manthiram, *Chem. Soc. Rev.* **2017**, *46*, 3006 – 3059; Q. Liu, X. Su, D. Lei, Y. Qin, J. G. Wen, F. M. Guo, Y. M. A. Wu, Y. C. Rong, R. H. Kou, X. H. Xiao, F. Aguesse, J. Bareno, Y. Ren, W. Q. Lu, Y. X. Li, *Nat. Energy* **2018**, *3*, 936 – 943; J. Lee, D. A. Kitchaev, D. H. Kwon, C. W. Lee, J. K. Papp, Y. S. Liu, Z. Lun, R. J. Clement, T. Shi, B. D. McCloskey, J. Guo, M. Balasubramanian, G. Ceder, *Nature* **2018**, *556*, 185 – 190.

[5] Y. Lu, J. Chen, *Nat. Rev. Chem.* **2020**, *4*, 127 – 142; C. Yang, J. Chen, X. Ji, T. P. Pollard, X. Lü, C.-J. Sun, S. Hou, Q. Liu, C. Liu, T. Qing, Y. Wang, O. Borodin, Y. Ren, K. Xu, C. Wang, *Nature* **2019**, *569*, 245 – 250; L. Suo, O. Borodin, T. Gao, M. Olguin, J. Ho, X. Fan, C. Luo, C. Wang, K. Xu, *Science* **2015**, *350*, 938 – 943.

[6] M. Li, C. Wang, Z. Chen, K. Xu, J. Lu, *Chem. Rev.* **2020**, *120*, 6783 – 6819.

[7] K. Xu, *Chem. Rev.* **2014**, *114*, 11503 – 11618.

[8] K. Xu, Y. F. Lam, S. S. Zhang, T. R. Jow, T. B. Curtis, *J. Phys. Chem. C* **2007**, *111*, 7411 – 7421; X. Q. Zhang, X. Chen, X. B. Cheng, B. Q. Li, X. Shen, C. Yan, J. Q. Huang, Q. Zhang, *Angew. Chem. Int. Ed.* **2018**, *57*, 5301 – 5305; *Angew. Chem.* **2018**, *130*, 5399 – 5403.

[9] A. von Cresce, K. Xu, *Electrochem. Solid-State Lett.* **2011**, *14*, A154 – A156; A. von Wald Cresce, O. Borodin, K. Xu, *J. Phys. Chem. C* **2012**, *116*, 26111 – 26117; K. Xu, *Nat. Sci. Rev.* **2017**, *4*, 19 – 20.

[10] J. Zheng, J. A. Lochala, A. Kwok, Z. D. Deng, J. Xiao, *Adv. Sci.* **2017**, *4*, 1700032; Y. Yamada, J. H. Wang, S. Ko, E. Watanabe, A. Yamada, *Nat. Energy* **2019**, *4*, 269 – 280.

[11] K. Sodeyama, Y. Yamada, K. Aikawa, A. Yamada, Y. Tateyama, *J. Phys. Chem. C* **2014**, *118*, 14091 – 14097.

[12] L. Suo, D. Oh, Y. Lin, Z. Zhuo, O. Borodin, T. Gao, F. Wang, A. Kushima, Z. Wang, H. C. Kim, Y. Qi, W. Yang, F. Pan, J. Li, K. Xu, C. Wang, *J. Am. Chem. Soc.* **2017**, *139*, 18670 – 18680.

[13] Y. Yamada, K. Furukawa, K. Sodeyama, K. Kikuchi, M. Yaegashi, Y. Tateyama, A. Yamada, *J. Am. Chem. Soc.* **2014**, *136*, 5039 – 5046; J. Qian, W. A. Henderson, W. Xu, P. Bhattacharya, M. Engelhard, O. Borodin, J. G. Zhang, *Nat. Commun.* **2015**, *6*, 6362.

[14] S. Chen, J. Zheng, D. Mei, K. S. Han, M. H. Engelhard, W. Zhao, W. Xu, J. Liu, J. G. Zhang, *Adv. Mater.* **2018**, *30*, 1706102.

[15] X. D. Ren, S. R. Chen, H. Lee, D. H. Mei, M. H. Engelhard, S. D. Burton, W. G. Zhao, J. M. Zheng, Q. Y. Li, M. S. Ding, M. Schroeder, J. Alvarado, K. Xu, Y. S. Meng, J. Liu, J. G. Zhang, W. Xu, *Chem* **2018**, *4*, 1877 – 1892; X. H. Zhang, L. F. Zou, Y. B. Xu, X. Cao, M. H. Engelhard, B. E. Matthews, L. R. Zhong, H. P. Wu, H. Jia, X. D. Ren, P. Y. Gao, Z. H. Chen, Y. Qin, C. Kompella, B. W. Arey, J. Li, D. Y. Wang, C. M. Wang, J. G. Zhang, W. Xu, *Adv. Energy Mater.* **2020**, *10*, 2000368.

[16] X. Chen, X.-Q. Zhang, H.-R. Li, Q. Zhang, *Batteries Supercaps* **2019**, *2*, 128 – 131.

[17] C. Zhang, K. Ueno, A. Yamazaki, K. Yoshida, H. Moon, T. Mandai, Y. Umebayashi, K. Dokko, M. Watanabe, *J. Phys. Chem. B* **2014**, *118*, 5144 – 5153; K. Ueno, R. Tatara, S. Tsuzuki, S. Saito, H. Doi, K. Yoshida, T. Mandai, M. Matsugami, Y. Umebayashi, K. Dokko, M. Watanabe, *Phys. Chem. Chem. Phys.* **2015**, *17*, 8248 – 8257.

[18] Y. Yamada, M. Yaegashi, T. Abe, A. Yamada, *Chem. Commun.* **2013**, *49*, 11194 – 11196.

[19] X. Bogle, R. Vazquez, S. Greenbaum, A. Cresce, K. Xu, *J. Phys. Chem. Lett.* **2013**, *4*, 1664 – 1668.

[20] Y. Yamada, Y. Koyama, T. Abe, Z. Ogumi, *J. Phys. Chem. C* **2009**, *113*, 8948 – 8953; S.-K. Jeong, M. Inaba, Y. Iriyama, T. Abe, Z. Ogumi, *J. Power Sources* **2008**, *175*, 540 – 546.

[21] E. Peled, S. Menkin, *J. Electrochem. Soc.* **2017**, *164*, A1703 – A1719.

[22] S. K. Heiskanen, J. Kim, B. L. Lucht, *Joule* **2019**, *3*, 2322 – 2333.

[23] K. Xu, A. von Cresce, U. Lee, *Langmuir* **2010**, *26*, 11538 – 11543; K. Xu, *J. Electrochem. Soc.* **2007**, *154*, A162 – A167.

[24] F. Sagane, T. Abe, Z. Ogumi, *J. Phys. Chem. C* **2009**, *113*, 20135 – 20138.

Manuscript received: August 21, 2020
Revised manuscript received: September 22, 2020
Accepted manuscript online: September 25, 2020
Version of record online: November 19, 2020